Bulletin of the Geological Survey of Japan, vol. 74 (3), p. 155–166, 2023

Report

Constraint on the spatial distribution of the Early and Middle Jurassic units within the Nakatsugawa Complex of the North Kitakami Belt by detrital zircon U–Pb dating

OSAKA Masashi[1], AOKI Shogo[2, 3, *], UCHINO Takayuki[4] and FUKUYAMA Mayuko[5]

OSAKA Masashi, AOKI Shogo, UCHINO Takayuki and FUKUYAMA Mayuko (2023) Constraint on the spatial distribution of the Early and Middle Jurassic units within the Nakatsugawa Complex of the North Kitakami Belt by detrital zircon U–Pb dating. *Bulletin of the Geological Survey of Japan*, vol. 74 (3), p. 155–166, 6 figs, 3 tables.

Abstract: Previous detrital zircon U–Pb and fossil studies of the terrigenous rocks in the southwestern unit (Nakatsugawa Complex) of the North Kitakami Belt have suggested that the unit was formed during the Early to Middle Jurassic. In this study, we additionally performed detrital zircon U–Pb dating of two sandstones in the southwest part of the Nakatsugawa Complex (sample OM-07 and OM-06) for constraining the spatial distribution of the Early and Middle Jurassic units of the complex. As a result, those two samples showed youngest cluster ages of the middle and late Early Jurassic (183.3 ± 1.0 Ma in OM-07 and 176.7 ± 1.6 Ma in OM-06), respectively. Combining data from this and previous studies, we conclude that the unit from the southwestern margin to the location of OM-06 in the complex was formed during the Early Jurassic, while its northeastern part was formed during the Middle Jurassic. Moreover, it seems that the Nakatsugawa Complex has been formed without a significant age gap.

Keywords: North Kitakami Belt, accretionary age, detrital zircon, U–Pb dating, LA-ICP-MS

1. Introduction

The Kitakami Mountains, located on the Pacific side of the Tohoku Region, contain geological units formed in the Asian continental margin during the early Paleozoic to the late Mesozoic (Fig. 1). The southern half consists of the South Kitakami Belt composed of pre-Silurian basement rocks and Silurian–Early Cretaceous shallow marine deposits, while the northern half consists of the North Kitakami Belt composed mainly of Jurassic accretionary complexes. Between the two geologic belts, there is the Nedamo Belt composed of early Carboniferous and Early Triassic accretionary complexes (Uchino, 2021a).

In the North Kitakami Belt of the mountains, age-diagnostic fossils have been reported from pelagic sedimentary rocks of chert and limestone at several sites since the 1950s (e.g., Onuki, 1956). Those data suggest that the age of oceanic rocks within the southwest part of the belt is older than that of the northeast part (e.g., Ehiro *et al.*, 2008).

On the other hand, the accretionary ages of the belt indicated by fossils and detrital zircon U–Pb ages from the terrigenous clastic rocks show a geochronological younging polarity from the southwest to the northeast (Suzuki *et al.*, 2007; Ehiro *et al.*, 2008), and vary from the Late Triassic to the Early Cretaceous (e.g., Matsuoka, 1988; Uchino, 2017, 2019, 2021b; Ueda *et al.*, 2018; Uchino and Suzuki, 2020). In addition, Nakae and Kurihara (2011) indicated the presence of a late Permian accretionary complex in the western margin of the North Kitakami Belt in the Kamaishi area.

In the Nakatsugawa Complex of the Sotoyama district, the southwestern margin of the North Kitakami Belt, detrital zircon U–Pb and radiolarian fossil studies of the terrigenous rocks also show a younger accretionary age within this unit toward the northeast, from the Early to the Middle Jurassic (Fig. 2; Uchino, 2019, 2021b; Uchino and Suzuki, 2021).

For this study, we collected additional sandstone samples in this complex, and conducted detrital zircon

[1] Faculty of International Resource Sciences, Akita University, Akita 010-8502, Japan
[2] Graduate School of International Resource Sciences, Akita University, Akita 010-8502, Japan
[3] AIST, Geological Survey of Japan, Research Institute for Geo-Resources and Environment
[4] AIST, Geological Survey of Japan, Research Institute of Geology and Geoinformation
[5] Graduate School of Engineering Science, Akita University, Akita 010-8502, Japan
[*] Corresponding author: AOKI, S., Email: s-aoki@gipc.akita-u.ac.jp

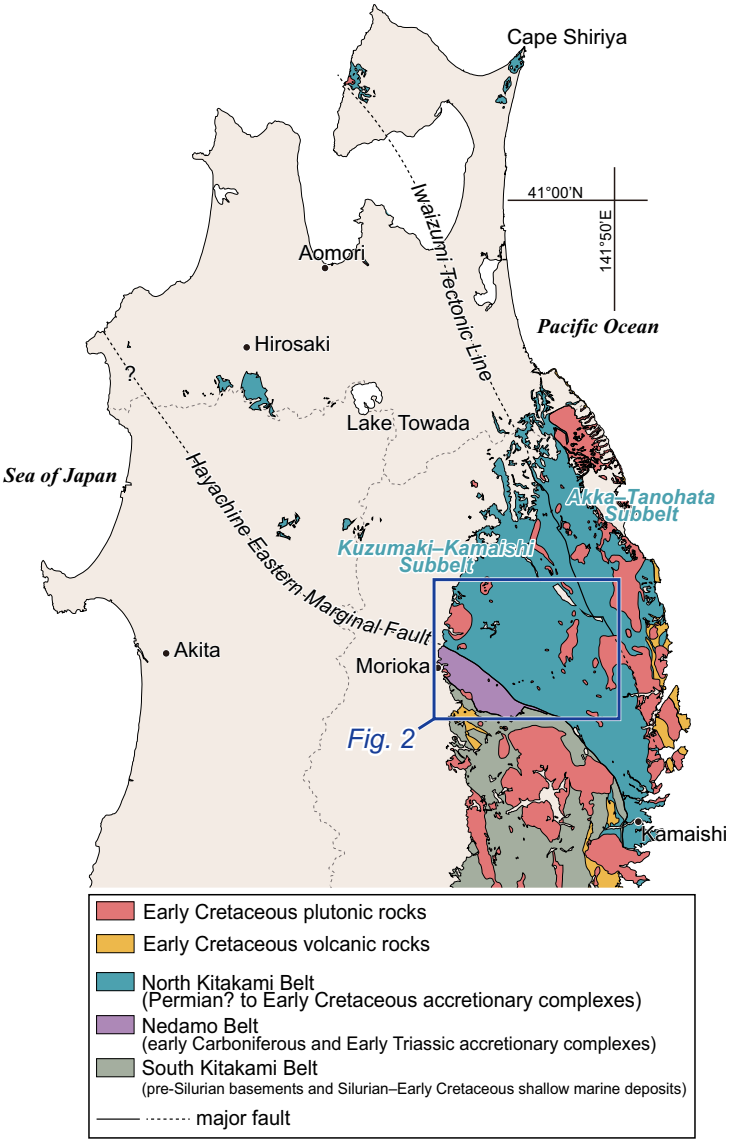

Fig. 1 Geological map showing the distribution of the North Kitakami Belt, the South Kitakami Belt and the Nedamo Belt with the intruding Early Cretaceous igneous rocks in Northeast Japan. This map was modified from the Seamless Digital Geological Map of Japan (1:200,000) V2 of the Geological Survey of Japan, AIST (2022). Colorless and pale beige areas show water areas and Cenozoic geologic bodies, respectively. Gray dashed line is a prefectural border.

U–Pb datings. The result of the U–Pb datings constrains the spatial distribution of the Early and Middle Jurassic accretionary complexes within the Nakatsugawa Complex.

2. Geological Outline

The North Kitakami Belt is composed mainly of the Jurassic accretionary complexes that occupy the northernmost part of Honshu in the Japanese Islands, and is most exposed in the northern part of the Kitakami Mountains (Fig. 1). In the Kitakami Mountains, the belt in contact with the Nedamo Belt on the southwestern side and the South Kitakami Belt on the southeastern side by the Hayachine Eastern Marginal Fault. It is further divided into the Kuzumaki–Kamaishi Subbelt on the west and the Akka–Tanohata Subbelt on the east by the Iwaizumi Tectonic Line based on differences of lithofacies and presence or absence of Paleozoic fossils from pelagic sediments (e.g., Okami and Ehiro, 1988; Ehiro *et al.*, 2008).

The Sotoyama district in Iwate Prefecture is located in the southwestern part of the Kuzumaki–Kamaishi Subbelt (Figs. 1, 2). In this area, an accretionary complex called the Nakatsugawa Complex is distributed (Uchino *et al.*, 2008). The southern limit of the complex is the boundary with the Nedamo Belt, while its northern and eastern limits are not defined. The Nakatsugawa Complex is composed mainly of laminated mudstone, sandstone, mudstone, thin alternation of sandstone and mudstone, and chert, with small amounts of basalt and limestone (Uchino, 2019). They have experienced significant shear deformation, and the clastic rocks in particular show well-developed bedding-parallel cleavages. The formations generally strike northwest-southeast and dip steeply to the southwest. On the other hand, small-scale synforms and antiforms with closed limbs of 100–200 m half-wavelength are locally developed around the southwestern margin of this area.

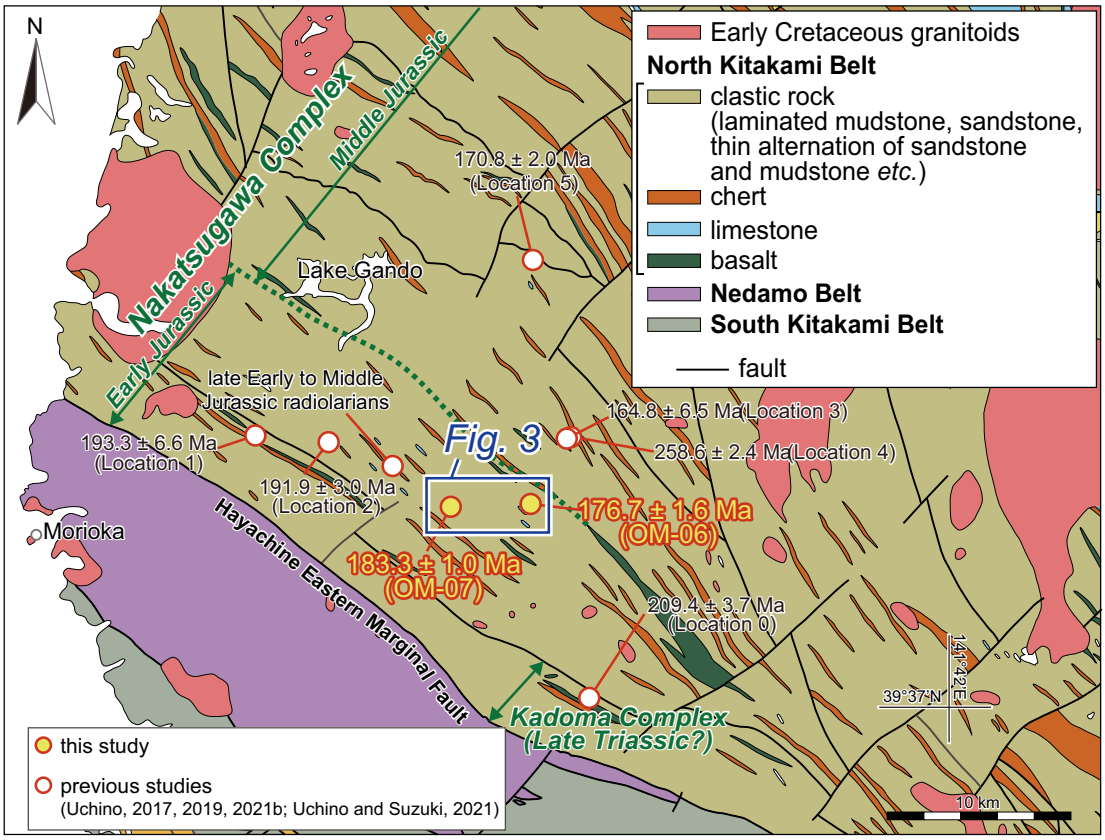

Fig. 2 Geological map of the southwestern margin of the North Kitakami Belt modified from the Seamless Digital Geological Map of Japan (1:200,000) V2 of the Geological Survey of Japan, AIST (2022). The locations of the sandstone samples in this and previous studies are shown with the youngest cluster ages of the zircons based on the YC2σ method of Dickinson and Gehrels (2009). Green dotted line is the boundary between the Early and Middle Jurassic systems.

Uchino (2019, 2021b) performed LA-ICP-MS U–Pb dating of detrital zircons from five sandstones in this complex. The youngest cluster ages based on the YC2σ method of Dickinson and Gehrels (2009) are 193.3 ± 6.6 Ma (Location 1 in Fig. 2), 191.9 ± 3.0 Ma (Location 2), 164.8 ± 6.5 Ma (Location 3), 258.6 ± 2.4 Ma (Location 4), and 170.8 ± 2.0 Ma (Location 5), respectively. Moreover, in the Kadoma Complex located southeast of the Nakatsugawa Complex, tuffaceous mudstone (Location 0) shows the youngest cluster age of 209.4 ± 3.7 Ma (Uchino, 2017). Those data, except for the U–Pb data of the sandstone in Location 4, suggest that the accretionary ages of the Nakatsugawa and Kadoma complexes vary from the Late Triassic, the Early Jurassic to the Middle Jurassic in a northeast direction (Fig. 2). It is also supported by the paleontological research of the mudstone located between the sandstone outcrops in Locations 2 and 3 yielding radiolarian fossils of the late Early to Middle Jurassic (Uchino and Suzuki, 2021).

3. Sample Description

For this study, two sandstone samples, OM-07 and OM-06, were collected in the Sotoyama district. They are located between the sandstone outcrops of Locations 2 and 3 studied by Uchino (2019, 2021b) in terms of geologic structure (Figs. 2, 3). Sample OM-07 was collected from a tributary (Todomatsu Stream) of the Hiegara Stream (Location: 39°43'03.60" N, 141°24'40.35" E). Sample OM-06 was collected from a tributary (Sannomata Stream) of the Okawa River in the southwesternmost area of Iwaizumi Town, ca. 3 km east of the location of OM-07 (Location: 39°43'11.13" N, 141°27'17.51" E).

They are medium sandstones showing slaty cleavage structures (Fig. 4a, b). They consist of quartz and plagioclase with subordinate amounts of K-feldspar and lithic fragments. Some of the quartz grains show wavy extinction, and most of the plagioclase are saussuritized. In OM-06, most of those grains are deformed into elliptical shapes or elongated, defining the foliation of the rocks (Fig. 4b). Moreover, in the sample, pressure solution cleavages are observed between the grains. Rock types of the many lithic fragments are difficult to identify due to deformation and alteration, but the few recognizable ones are chert and mudstone. Sericite, titanite, epidote, muscovite and zircon were also recognized as accessory minerals. Sericite

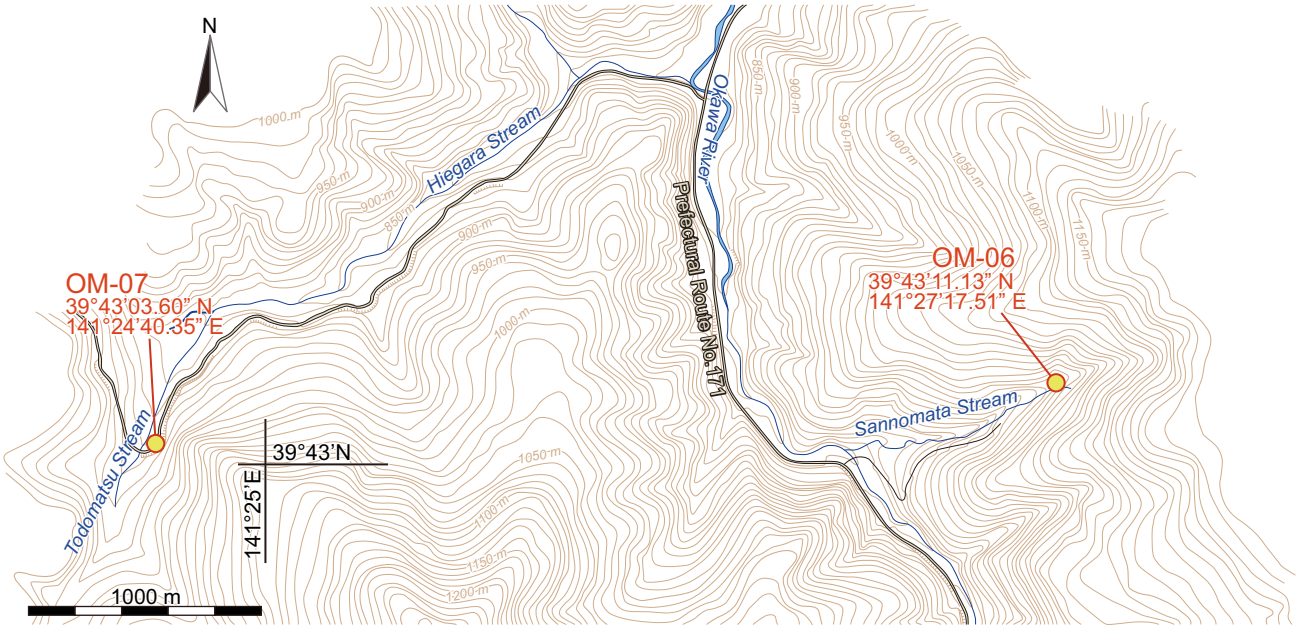

Fig. 3 Locations of the sandstone samples of OM-07 and OM-06 for zircon U–Pb dating. The topographic map is modified from the GSI map (https://maps.gsi.go.jp/, Accessed: 2022-8-10) of the Geospatial Information Authority of Japan.

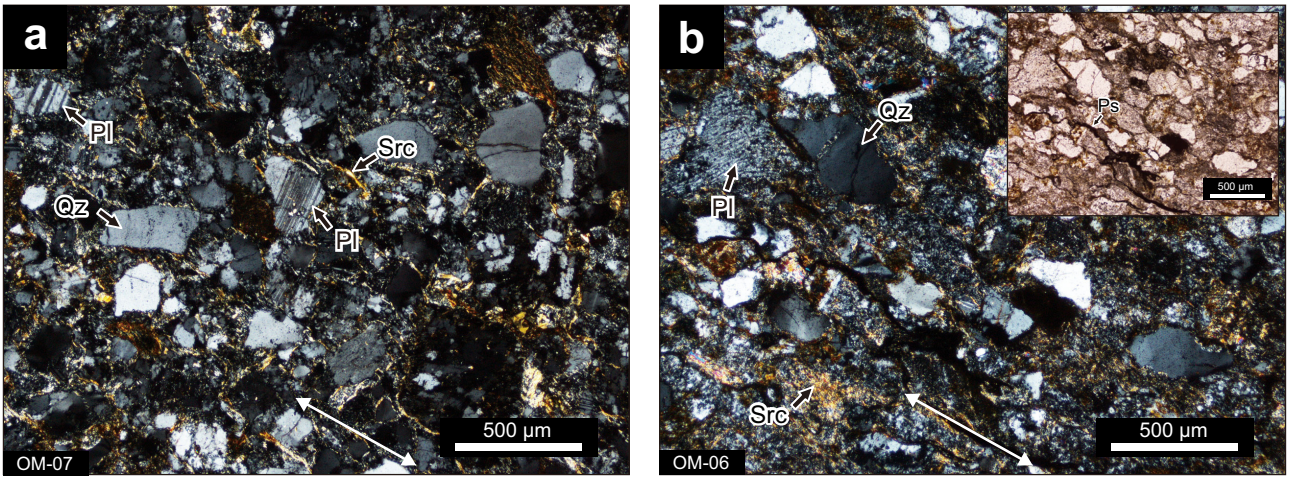

Fig. 4 Thin-section photomicrographs of the sandstones from (a) OM-07 and (b) OM-06. White arrows indicate the direction of the cleavage plane.
Mineral abbreviations: Qz, quartz; Pl, Plagioclase; Src, sericite; Ps, Pressure solution cleavage

occurs along the cleavage plane.

4. Analytical methods

Approximately 5 kg of each sample was crushed into fragments in a stainless-steel mortar, which were subsequently passed through a sieve with a 250-μm opening. Subsequently, zircons were concentrated by conventional panning and magnetic separation. Finally, the separated zircon grains were mounted on a 5-mm acrylic disc, and polished.

The cathodoluminescence (CL) imaging of the zircons was performed at Akita University, using a JSM-6610LV scanning electron microscope (JEOL, Ltd., Tokyo, Japan) combined with a Mini-CL detector (Gatan, Inc., California, United States). The analytical conditions were an acceleration voltage of 20 kV and a beam current of 2–5 nA. Most zircons exhibit oscillatory zonings from core to rim in CL images, suggesting that they were crystallized from magma (Fig. 5; e.g., Corfu *et al.*, 2003).

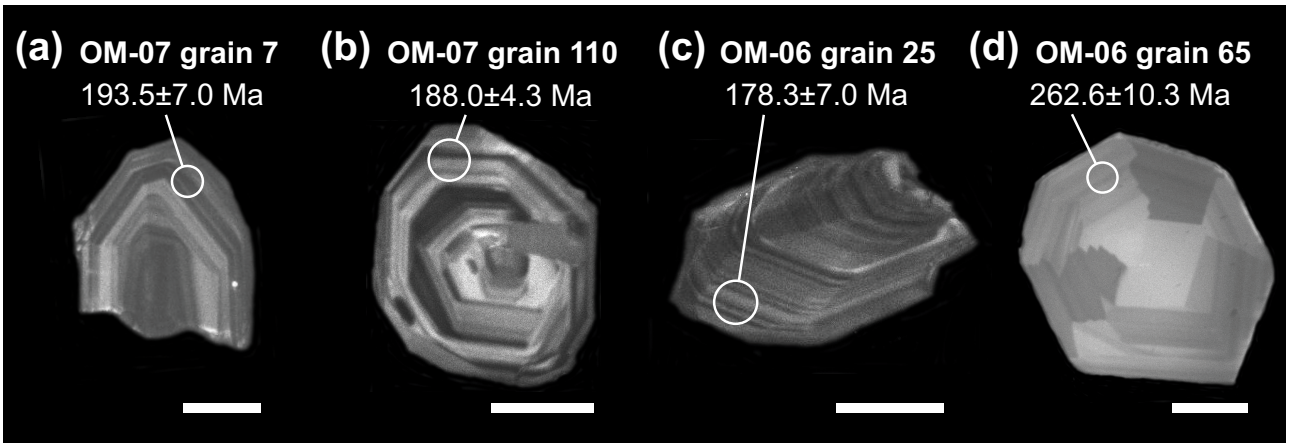

Fig. 5 Cathodoluminescence (CL) images of the representative detrital zircons from (a, b) OM-07 and (c, d) OM-06. Scale bars are 50 μm.

In situ zircon U–Pb dating was carried out at Akita University using an Agilent 7700x quadrupole ICP-MS (Agilent Technologies, Inc., California, United States) coupled to an NWR-193UC laser ablation (LA) system that utilizes a 193 nm ArF excimer laser (ESI, Inc., Oregon, United States). The detailed analytical methods are shown in Table 1.

The discs of zircons were set in the two-volume sample cell of the LA system. The areas in zircons showing oscillatory zonings with no fractures or inclusions were selected for the analysis referring to the LA camera and the CL images of the zircons. The selected ones were ablated for 30 seconds by the laser with fluence of 7.20 J/cm^2, repetition rate of 5 Hz, and laser spot size diameter of 20 μm. The ablated materials were carried to the ICP-MS with He gas, which was introduced into the two-volume sample chamber and cup. On the ICP-MS, six nuclides (^{202}Hg, ^{204}Pb, ^{206}Pb, ^{207}Pb, ^{208}Pb, ^{232}Th, and ^{238}U) were analyzed.

Data were acquired for groups of 20 spot analyses of unknown zircon grains including a secondary standard bracketed by three spot analyses of the 91500 zircon reference material (Wiedenbeck *et al.*, 1995), which was measured for corrections of Pb/U and Pb isotopic ratios. All uncertainties are quoted at a 2-sigma level. As measured counts of ^{204}Pb after the correction of ^{204}Hg by ^{202}Hg are small, no common Pb correction is applied.

Concordance is defined as values of 100 % × [(^{207}Pb/^{235}U age) − (^{206}Pb/^{238}U age)]/(^{207}Pb/^{235}U age), and age data with the concordance range from −10 % to +10 % are adopted as concordant data.

Throughout all the analyses, the Plešovice zircon (337.13 Ma ± 0.37 Ma: Sláma *et al.*, 2008) was also analyzed as a secondary standard for quality control. The 28 analyses yielded a weighted mean ^{206}Pb/^{238}U age of 341.7 Ma ± 1.8 Ma (95 % conf., MSWD = 0.55) and ^{207}Pb/^{235}U age of 337.5 Ma ± 2.3 Ma (95 % conf., MSWD = 0.42).

Table 1 Analytical condition of LA-ICP-MS for zircon U–Pb dating.

Laser ablation system	
Model	NWR-193UC (made by New Wave Research, Inc.)
Cell type	TruLine cell
Laser type	Excimer ArF
Wave length	193 nm
Energy density (Fluence)	7.20 J/cm^2
Spot diameter	20 μm
Repetition rate	5 Hz
Duration of laser ablation	30 sec
Sampling mode/pattern	Static spot ablation
Carrier He gas flow	
Cell cup gas	0.10–0.15 l/min
Cell base gas	0.52–0.55 l/min
Smoother	ESI signal smoother
ICP-MS system	
Model	Agilent 7700 (made by Agilent Technologies, Inc.)
ICP-MS type	Quadrupole
RF power	1600 W
Ar gas flow rate	
Nebulizer gas	0.66–0.68 l/min
Dilution gas	0.68 l/min
Auxiliary gas	0.90 l/min
Plasma gas	15.0 l/min
Masses measured	^{202}Hg, ^{204}Pb, ^{206}Pb, ^{207}Pb, ^{208}Pb, ^{232}Th and ^{238}U
Integration time per peak	0.02 sec for ^{202}Hg, ^{204}Pb, ^{232}Th and ^{238}U; 0.04 sec for ^{206}Pb and ^{208}Pb; 0.08 sec for ^{207}Pb
Total time of one mass scan cycle	0.2520 sec
Oxide production rate (^{238}U^{16}O$^+$/^{238}U$^+$)	<1 %
Doubly-charged ion production rate (^{44}Ca^{2+}/^{44}Ca$^+$)	<1 %
Standards	
Primary standard	Nancy 91500 (Wiedenbeck *et al*., 1995)
Secondary standard	Prešovice (Sláma *et al*., 2008)

Table 2 Zircon U–Pb isotopic data for OM-07.

Grain number	Isotopic ratios						Age (Ma)						Th/U	Remarks
	$^{207}Pb/^{206}Pb$	± error 2σ	$^{206}Pb/^{238}U$	± error 2σ	$^{207}Pb/^{235}U$	± error 2σ	$^{206}Pb/^{238}U$	± error 2σ	$^{207}Pb/^{235}U$	± error 2σ	$^{207}Pb/^{206}Pb$	± error 2σ		
grain1	0.0578	0.1016	0.0438	0.0269	0.3399	0.0897	276.1	14.6	297.1	46.2			0.67	
grain2	0.0479	0.0555	0.0407	0.0250	0.2652	0.0512	256.9	12.6	238.9	21.8			0.55	
grain3	0.0503	0.0535	0.0320	0.0216	0.2198	0.0510	203.1	8.6	201.7	18.7			0.57	
grain4	0.0431	0.1584	0.0458	0.0386	0.2719	0.1485	288.9	21.8	244.2	64.6			0.34	*dis.*
grain5	0.0544	0.0331	0.0301	0.0128	0.2251	0.0392	191.0	4.8	206.1	14.6			0.53	
grain6	0.0572	0.0716	0.0283	0.0262	0.2215	0.0695	179.9	9.3	203.1	25.6			0.53	*dis.*
grain7	0.0492	0.0253	0.0305	0.0183	0.2052	0.0235	193.5	7.0	189.5	8.1			0.62	
grain8	0.0483	0.0285	0.0296	0.0111	0.1962	0.0250	188.3	4.1	181.9	8.3			0.41	
grain11	0.0485	0.0531	0.0391	0.0176	0.2607	0.0565	247.4	8.6	235.2	23.7			0.62	
grain14	0.0453	0.0514	0.0289	0.0253	0.1781	0.0486	183.5	9.2	166.4	14.9			0.70	*
grain15	0.0536	0.0379	0.0419	0.0259	0.3047	0.0230	264.4	13.4	270.0	10.9			0.76	
grain16	0.0476	0.0537	0.0401	0.0209	0.2618	0.0552	253.2	10.4	236.1	23.3			0.41	
grain17	0.0546	0.1080	0.0311	0.0372	0.2260	0.0919	197.5	14.5	206.9	34.4			0.52	*
grain18	0.0488	0.0357	0.0295	0.0141	0.1975	0.0342	187.7	5.2	183.0	11.5			0.58	*
grain19	0.0644	0.0535	0.0454	0.0284	0.3990	0.0508	286.4	15.9	340.9	29.4			0.46	*dis.*
grain20	0.0461	0.1222	0.0426	0.0426	0.2641	0.1204	269.2	22.5	237.9	51.1			0.58	*dis.*
grain22	0.1138	0.0092	0.3269	0.0112	5.1055	0.0127	1823.3	35.5	1837.0	21.7	1873.5	33.3	0.58	
grain23	0.0539	0.0521	0.0420	0.0176	0.3098	0.0507	265.3	9.1	274.0	24.4			0.42	
grain24	0.0485	0.0303	0.0283	0.0169	0.1885	0.0322	180.2	6.0	175.4	10.4			0.54	*
grain25	0.0495	0.0478	0.0279	0.0182	0.1891	0.0471	177.2	6.4	175.8	15.2			0.64	*
grain27	0.0488	0.0561	0.0423	0.0205	0.2805	0.0485	267.0	10.7	251.1	21.6			0.74	
grain28	0.0498	0.0234	0.0300	0.0184	0.2056	0.0309	190.8	6.9	189.8	10.7			0.99	
grain29	0.0622	0.1503	0.0462	0.0392	0.3779	0.1223	291.3	22.3	325.5	68.2			0.61	*dis.*
grain31	0.0470	0.0468	0.0366	0.0132	0.2353	0.0429	231.4	6.0	214.6	16.6			0.62	
grain33	0.0512	0.0603	0.0353	0.0226	0.2472	0.0595	223.7	9.9	224.3	23.9			0.60	
grain34	0.0509	0.0778	0.0414	0.0210	0.2870	0.0724	261.3	10.7	256.2	32.8			0.76	
grain35	0.1157	0.0142	0.3289	0.0170	5.2229	0.0202	1833.2	54.4	1856.4	34.4	1903.8	51.0	0.23	
grain36	0.0531	0.0809	0.0425	0.0266	0.3093	0.0843	268.2	14.0	273.7	40.5			0.99	
grain37	0.0513	0.0473	0.0412	0.0219	0.2889	0.0431	260.6	11.2	257.7	19.6			0.70	
grain39	0.0532	0.0488	0.0313	0.0218	0.2275	0.0505	198.7	8.5	208.1	19.0			0.52	
grain40	0.1126	0.0277	0.3320	0.0100	5.1253	0.0253	1848.1	32.1	1840.3	43.0	1854.6	100.4	2.29	
grain41	0.0474	0.0464	0.0329	0.0160	0.2137	0.0480	208.7	6.6	196.6	17.2			0.57	
grain43	0.1108	0.0181	0.3409	0.0101	5.1822	0.0176	1890.8	33.1	1849.7	30.0	1825.7	65.6	1.44	
grain44	0.0532	0.0675	0.0406	0.0287	0.2943	0.0617	256.8	14.5	262.0	28.5			0.44	
grain50	0.1151	0.0146	0.3472	0.0156	5.4840	0.0195	1921.5	51.7	1898.1	33.5	1894.0	52.7	0.27	
grain51	0.0413	0.0497	0.0328	0.0222	0.1857	0.0517	208.1	9.1	172.9	16.4			0.72	*dis.*
grain52	0.0573	0.0536	0.0411	0.0182	0.3226	0.0537	259.4	9.3	283.9	26.6			1.30	
grain53	0.0532	0.0586	0.0295	0.0205	0.2135	0.0512	187.2	7.6	196.5	18.3			0.46	*
grain56	0.1139	0.0124	0.3309	0.0133	5.1771	0.0167	1842.9	42.5	1848.9	28.5	1876.5	44.8	0.44	
grain57	0.0551	0.0900	0.0289	0.0394	0.2117	0.0732	183.5	14.3	195.0	26.0			0.54	*
grain60	0.0459	0.1413	0.0417	0.0383	0.2563	0.1350	263.3	19.8	231.6	56.0			0.96	*dis.*
grain61	0.0497	0.0466	0.0277	0.0207	0.1882	0.0436	176.4	7.2	175.1	14.0			0.36	*
grain62	0.0447	0.0737	0.0407	0.0192	0.2472	0.0655	257.2	9.7	224.3	26.4			0.76	*dis.*
grain63	0.0583	0.1174	0.0320	0.0213	0.2536	0.1117	202.9	8.5	229.5	45.9			0.58	*dis.*

grain67	0.0524	0.0455	0.0295	0.0208	0.2109	0.0370	187.5	7.7	194.3	13.1			0.39	*
grain69	0.0511	0.0599	0.0329	0.0224	0.2273	0.0459	208.4	9.2	208.0	17.3			0.38	
grain71	0.0471	0.0643	0.0423	0.0159	0.2707	0.0515	266.9	8.3	243.3	22.3			0.82	
grain72	0.0533	0.0778	0.0460	0.0229	0.3316	0.0710	289.6	13.0	290.8	35.9			0.29	
grain73	0.0498	0.0642	0.0313	0.0190	0.2129	0.0605	198.5	7.4	196.0	21.6			0.69	
grain75	0.0479	0.0565	0.0431	0.0223	0.2814	0.0513	271.9	11.9	251.8	22.9			0.42	
grain76	0.0458	0.0367	0.0437	0.0251	0.2744	0.0416	275.7	13.5	246.2	18.2			0.71	*dis.*
grain77	0.1156	0.0152	0.3313	0.0113	5.2542	0.0130	1844.6	36.2	1861.5	22.2	1902.9	54.5	0.54	
grain78	0.0507	0.0724	0.0317	0.0252	0.2185	0.0653	201.4	10.0	200.7	23.8			0.59	
grain80	0.0514	0.0556	0.0325	0.0284	0.2284	0.0562	206.3	11.5	208.9	21.2			0.55	
grain82	0.0551	0.0595	0.0327	0.0161	0.2459	0.0500	207.7	6.6	223.3	20.1			0.50	
grain85	0.1104	0.0139	0.3529	0.0132	5.3446	0.0127	1948.3	44.4	1876.0	21.7	1820.1	50.6	0.21	
grain87	0.0523	0.0309	0.0419	0.0121	0.3007	0.0327	264.7	6.3	266.9	15.4			0.23	
grain88	0.0476	0.0360	0.0283	0.0164	0.1850	0.0393	180.0	5.8	172.4	12.5			0.39	*
grain91	0.0529	0.0523	0.0408	0.0307	0.2938	0.0523	257.9	15.5	261.5	24.1			0.42	
grain92	0.0458	0.0627	0.0301	0.0205	0.1883	0.0643	190.9	7.7	175.2	20.7			0.50	*
grain93	0.0517	0.0324	0.0408	0.0204	0.2885	0.0308	257.6	10.3	257.4	14.0			0.94	
grain102	0.0501	0.0474	0.0318	0.0153	0.2192	0.0511	202.1	6.1	201.3	18.7			0.53	
grain103	0.0512	0.0270	0.0282	0.0150	0.1981	0.0272	179.3	5.3	183.5	9.1			0.40	*
grain104	0.0501	0.0502	0.0331	0.0274	0.2249	0.0406	210.0	11.3	206.0	15.1			0.49	
grain106	0.0542	0.0480	0.0416	0.0233	0.3083	0.0459	262.8	12.0	272.9	22.0			0.81	
grain109	0.0493	0.0273	0.0460	0.0111	0.3113	0.0286	290.0	6.3	275.2	13.8			0.49	
grain110	0.0491	0.0340	0.0296	0.0117	0.1992	0.0334	188.0	4.3	184.4	11.3			0.68	
grain113	0.1090	0.0320	0.3417	0.0173	5.0975	0.0312	1895.0	56.8	1835.7	53.0	1795.5	116.9	1.59	
grain114	0.1130	0.0161	0.3416	0.0134	5.3002	0.0184	1894.5	43.8	1868.9	31.5	1862.2	58.3	0.09	
grain115	0.0547	0.0243	0.0411	0.0211	0.3077	0.0262	259.4	10.7	272.4	12.5			0.77	
grain118	0.0479	0.0363	0.0336	0.0138	0.2216	0.0414	213.3	5.8	203.2	15.2			0.79	
grain120	0.0526	0.0392	0.0299	0.0145	0.2155	0.0382	189.9	5.4	198.2	13.8			0.48	
grain121	0.1144	0.0121	0.3397	0.0114	5.3338	0.0113	1885.3	37.3	1874.3	19.3	1884.3	43.4	0.14	
grain122	0.0485	0.0479	0.0299	0.0200	0.1975	0.0447	189.6	7.5	183.0	15.0			0.47	*

Asterisk "*" indicates the data used for calculation of youngest cluster age. "*dis.*" indicates discordant data.

Table 3 Zircon U–Pb isotopic data for OM-06.

Grain	Isotopic ratios						Age (Ma)							
number	$^{207}Pb/^{206}Pb$	± error 2σ	$^{206}Pb/^{238}U$	± error 2σ	$^{207}Pb/^{235}U$	± error 2σ	$^{206}Pb/^{238}U$	± error 2σ	$^{207}Pb/^{235}U$	± error 2σ	$^{207}Pb/^{206}Pb$	± error 2σ	Th/U	Remarks
grain2	0.0457	0.0280	0.0323	0.0201	0.2024	0.0330	204.9	8.1	187.2	11.3			0.45	
grain3	0.0499	0.0413	0.0430	0.0214	0.2931	0.0420	271.3	11.4	261.0	19.3			0.61	
grain4	0.0468	0.0649	0.0316	0.0168	0.2031	0.0672	200.5	6.6	187.8	23.1			0.61	
grain5	0.0509	0.0455	0.0428	0.0189	0.2984	0.0465	270.1	10.0	265.1	21.7			0.93	
grain6	0.0468	0.0226	0.0320	0.0180	0.2052	0.0237	202.9	7.2	189.5	8.2			0.71	
grain7	0.0509	0.0408	0.0403	0.0143	0.2804	0.0370	254.6	7.1	251.0	16.5			0.65	
grain10	0.0548	0.0276	0.0413	0.0117	0.3098	0.0263	260.7	6.0	274.1	12.6			0.46	
grain11	0.0505	0.0230	0.0380	0.0113	0.2635	0.0250	240.4	5.3	237.5	10.6			0.21	
grain12	0.0485	0.0226	0.0424	0.0218	0.2811	0.0162	267.7	11.4	251.5	7.2			0.54	
grain13	0.0555	0.0266	0.0744	0.0171	0.5663	0.0289	462.6	15.2	455.6	21.2			0.68	
grain14	0.0496	0.0405	0.0295	0.0128	0.2006	0.0384	187.4	4.7	185.6	13.0			0.48	
grain16	0.0499	0.0302	0.0298	0.0146	0.2046	0.0348	189.6	5.5	189.0	12.0			0.48	
grain18	0.0510	0.0593	0.0430	0.0314	0.2999	0.0628	271.2	16.7	266.3	29.4			0.93	
grain25	0.0520	0.0223	0.0281	0.0199	0.1998	0.0217	178.3	7.0	185.0	7.3			0.26	*
grain26	0.0511	0.0161	0.0425	0.0103	0.2980	0.0168	268.2	5.4	264.8	7.8			0.42	
grain31	0.0450	0.0438	0.0316	0.0176	0.1957	0.0515	200.6	7.0	181.5	17.1			1.08	
grain32	0.0502	0.0282	0.0283	0.0131	0.1953	0.0310	179.9	4.6	181.2	10.3			0.58	*
grain35	0.0483	0.0480	0.0317	0.0201	0.2087	0.0409	201.2	8.0	192.5	14.4			0.59	
grain37	0.0550	0.0386	0.0405	0.0131	0.3040	0.0311	255.7	6.6	269.6	14.7			0.30	
grain38	0.0555	0.0364	0.0430	0.0161	0.3276	0.0362	271.5	8.6	287.7	18.1			0.71	
grain39	0.0507	0.0243	0.0316	0.0160	0.2199	0.0289	200.5	6.3	201.8	10.6			0.77	
grain40	0.0474	0.0656	0.0441	0.0246	0.2843	0.0646	277.9	13.4	254.1	29.0			0.63	
grain45	0.0442	0.0662	0.0311	0.0172	0.1879	0.0667	197.4	6.7	174.8	21.4			0.70	*dis.*
grain49	0.0598	0.0425	0.0410	0.0131	0.3372	0.0494	258.7	6.6	295.1	25.3			0.60	*dis.*
grain56	0.0530	0.0398	0.0466	0.0197	0.3392	0.0447	293.4	11.3	296.6	23.0			0.65	
grain61	0.0573	0.1324	0.0440	0.0402	0.3490	0.1429	277.3	21.8	304.0	75.2			0.44	
grain62	0.0490	0.0592	0.0338	0.0253	0.2249	0.0547	214.0	10.7	206.0	20.4			1.29	
grain64	0.0518	0.0385	0.0305	0.0221	0.2172	0.0444	193.7	8.5	199.6	16.1			0.50	
grain65	0.0519	0.0617	0.0416	0.0200	0.2955	0.0602	262.6	10.3	262.9	27.9			0.82	
grain66	0.0472	0.0335	0.0314	0.0155	0.2034	0.0352	199.3	6.1	188.0	12.1			0.52	
grain67	0.0486	0.0447	0.0353	0.0178	0.2361	0.0492	223.6	7.8	215.2	19.1			0.72	
grain69	0.1120	0.0153	0.3325	0.0119	5.1138	0.0184	1850.7	38.4	1838.4	31.2	1845.3	55.4	0.46	
grain70	0.0515	0.0383	0.0414	0.0117	0.2922	0.0345	261.8	6.0	260.3	15.8			0.65	
grain72	0.0523	0.0231	0.0406	0.0143	0.2914	0.0230	256.5	7.2	259.7	10.5			0.80	
grain73	0.0476	0.0593	0.0305	0.0172	0.2009	0.0679	193.8	6.6	185.9	23.1			0.57	
grain74	0.0564	0.0391	0.0417	0.0186	0.3222	0.0408	263.4	9.6	283.6	20.2			0.60	
grain75	0.0535	0.0261	0.0303	0.0167	0.2226	0.0282	192.5	6.3	204.0	10.4			0.37	
grain76	0.0498	0.0450	0.0309	0.0221	0.2112	0.0467	196.4	8.5	194.6	16.6			0.59	
grain79	0.0460	0.0490	0.0309	0.0163	0.1943	0.0443	195.9	6.3	180.3	14.6			0.52	
grain81	0.0515	0.0395	0.0421	0.0226	0.2975	0.0476	265.7	11.7	264.5	22.2			0.58	
grain85	0.1115	0.0078	0.3308	0.0144	5.0660	0.0168	1842.3	46.0	1830.4	28.5	1837.0	28.2	0.06	
grain86	0.0498	0.0410	0.0313	0.0160	0.2141	0.0436	198.7	6.3	197.0	15.6			0.62	
grain88	0.0540	0.0686	0.0417	0.0298	0.3072	0.0689	263.2	15.4	272.0	32.9			0.71	
grain89	0.1134	0.0094	0.3353	0.0120	5.2229	0.0135	1864.1	38.9	1856.4	23.1	1868.6	33.8	0.23	

grain90	0.0489	0.0353	0.0309	0.0149	0.2072	0.0324	196.4	5.8	191.2	11.3						0.61	
grain91	0.0483	0.0526	0.0293	0.0232	0.1943	0.0573	186.4	8.5	180.3	18.9						0.49	
grain93	0.0518	0.0369	0.0403	0.0162	0.2860	0.0321	254.9	8.1	255.4	14.5						0.43	
grain94	0.0525	0.0328	0.0396	0.0199	0.2847	0.0312	250.5	9.8	254.4	14.0						0.46	
grain95	0.0476	0.0364	0.0289	0.0147	0.1885	0.0377	183.4	5.3	175.4	12.1						0.49	
grain96	0.0479	0.0270	0.0351	0.0197	0.2306	0.0288	222.4	8.6	210.7	10.9						0.49	
grain97	0.0458	0.0628	0.0314	0.0229	0.1966	0.0623	199.3	9.0	182.3	20.8						0.97	
grain98	0.0500	0.0479	0.0388	0.0172	0.2665	0.0529	245.6	8.3	239.9	22.6						0.56	
grain100	0.0509	0.0270	0.0403	0.0136	0.2807	0.0218	254.5	6.8	251.2	9.7						0.64	
grain101	0.0513	0.0388	0.0410	0.0289	0.2873	0.0407	259.0	14.7	256.4	18.5						0.60	
grain102	0.0466	0.0575	0.0314	0.0283	0.1997	0.0558	199.3	11.1	184.9	18.9						0.70	
grain103	0.0522	0.0276	0.0410	0.0141	0.2930	0.0222	259.3	7.2	260.9	10.2						0.19	
grain106	0.0516	0.0162	0.0288	0.0124	0.2041	0.0209	183.0	4.5	188.6	7.2						0.66	
grain107	0.0502	0.0454	0.0418	0.0165	0.2867	0.0421	263.8	8.6	255.9	19.0						0.58	
grain108	0.0471	0.0309	0.0414	0.0160	0.2677	0.0336	261.6	8.2	240.9	14.4						0.83	
grain109	0.0555	0.0550	0.0415	0.0211	0.3153	0.0552	262.0	10.8	278.3	26.9						0.68	
grain110	0.1115	0.0108	0.3314	0.0103	5.0738	0.0123	1845.2	33.0	1831.7	20.9	1837.8	39.2				0.45	
grain112	0.0527	0.0630	0.0266	0.0189	0.1927	0.0644	169.5	6.3	178.9	21.1						0.68	*
grain113	0.0536	0.0448	0.0308	0.0164	0.2255	0.0410	195.5	6.3	206.5	15.3						0.86	
grain116	0.0451	0.0498	0.0345	0.0183	0.2130	0.0468	218.7	7.9	196.1	16.7						0.81	*dis.*
grain117	0.0504	0.0295	0.0389	0.0145	0.2688	0.0283	245.8	7.0	241.7	12.2						0.11	
grain119	0.0518	0.0222	0.0454	0.0122	0.3226	0.0198	286.2	6.8	283.9	9.8						0.82	
grain122	0.0467	0.0700	0.0419	0.0245	0.2667	0.0664	264.6	12.7	240.0	28.4						0.49	

Asterisk "*" indicates the data used for calculation of youngest cluster age. "*dis.*" indicates discordant data.

5. Result of U–Pb dating

The isotopic data of samples OM-07 and OM-06 are summarized in Tables 2 and 3, respectively.

For OM-07, 64 grains of the 74 zircon grains show concordant values. Of these, more than 80 % are dated to the Phanerozoic, and 11 grains are dated to the Proterozoic (2000 to 1800 Ma) (Fig. 6a). All of their Th/U ratios are over 0.1, which is characteristic of zircons crystallized from melts (e.g., Rubatto, 2002). The age histogram of the Phanerozoic zircons also shows a bimodal distribution with peaks around the middle Permian (270 to 260 Ma) and early Jurassic (200 to 180 Ma). The youngest age is 176.4 ± 7.2 Ma (grain 61). The youngest cluster age based on the YC2σ method is 183.3 ± 1.0 Ma (grain n = 13, MSWD = 2.3).

Of the 67 zircons measured in OM-06, 64 grains are concordant in age, with more than 90 % of the zircons dated to the Phanerozoic and only four to the Proterozoic (1900 to 1800 Ma). Except for the grain 85, their Th/U ratios exceed 0.1, which are characteristics of zircons crystallized from melts (e.g., Rubatto, 2002). Focusing on the Phanerozoic zircons, their $^{206}Pb/^{238}U$ age histogram shows a bimodal distribution with peaks around the middle Permian (270 to 260 Ma) and Early Jurassic (200 to 190 Ma) (Fig. 6b), and only one grain (grain 13) shows the Ordovician age (462.6 ± 15.2 Ma). The youngest age is 169.5 ± 6.3 Ma (grain 112). The youngest cluster age based on the YC2σ method of Dickinson and Gehrels (2009) is 176.7 ± 1.6 Ma (grain n = 3, MSWD = 3.7).

6. Discussion about the depositional age of OM-07 and OM-06

The youngest age of detrital zircons could constrain the maximum depositional age of the clastic rocks (e.g., Brown and Gehrels, 2007). In particular, if there has been active zircon-forming felsic magmatism with eruptions in the backland, the youngest cluster age is considered to be approximately the same as the true depositional age of the clastic rocks, because detrital zircons from newly-formed felsic volcanic rocks could be supplied to the trench in a short time (Sharman and Malkowski, 2020).

Geochronological studies of the felsic rocks in the Korean Peninsula indicate that the granitic formation was active in the Asian continental margin during the Early to Middle Jurassic (e.g., Sagong *et al.*, 2005; Kiminami and Imaoka, 2013; Kim *et al.*, 2015) while the Nakatsugawa Complex was formed. In addition, the contemporaneous felsic volcaniclastics associated with the granitic activities must have also been formed in large quantities, even though most of them may have been lost probably due to surface erosion (e.g., Han *et al.*, 2006).

Both OM-07 and OM-06 show the youngest cluster ages of the Early Jurassic. Considering above the felsic magmatic history in the Asian continental margin, their youngest cluster ages could represent their depositional

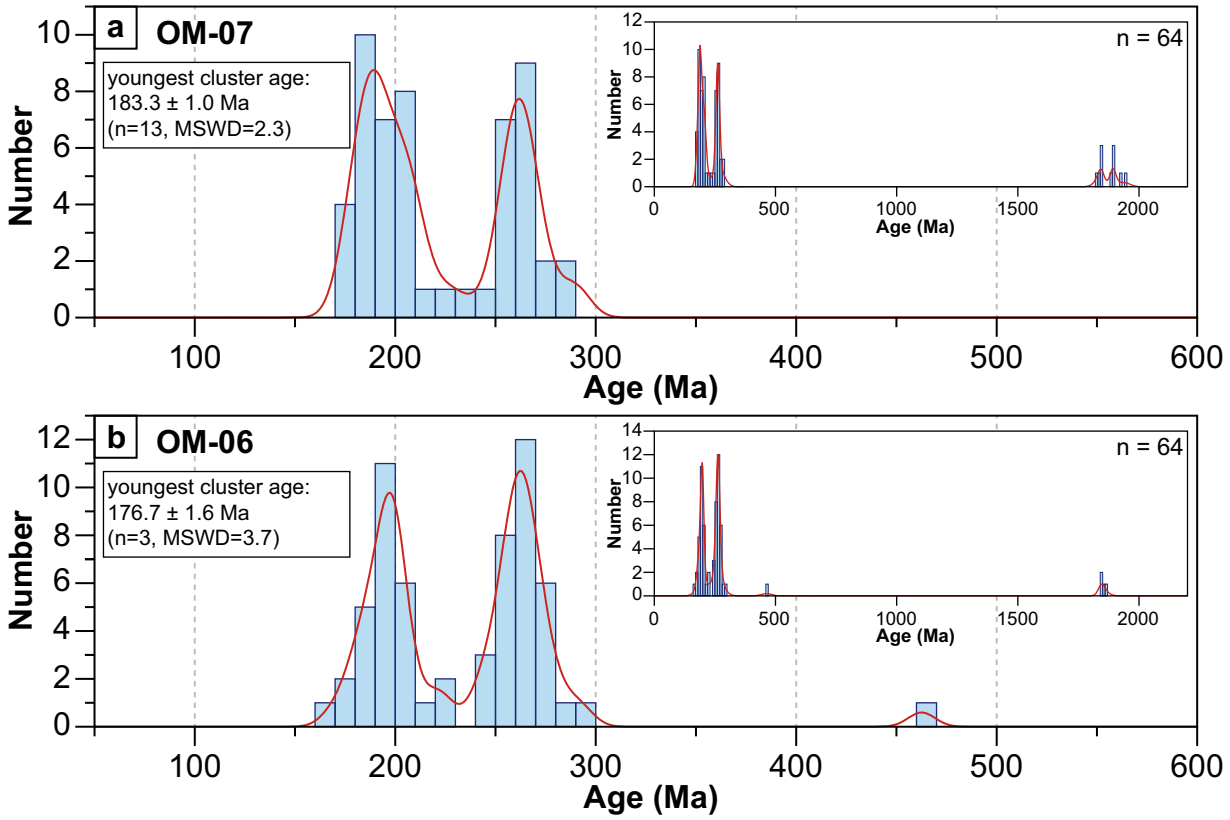

Fig. 6 Age histograms of the concordant data with Kernel Density Estimation (KDE) plots for (a) OM-07 and (b) OM-06 made with Isoplot R (Vermeesch, 2018). The horizontal axis indicates $^{206}Pb/^{238}U$ age. n: number of data

ages, i.e., the sandstones of OM-07 and OM-06 were deposited in the Early Jurassic.

Moreover, they show the same bimodal age distributions with peaks around the middle Permian and the Early Jurassic as the sandstones in Locations 1 and 2 of the Nakatsugawa Complex which were deposited in the Early Jurassic (Uchino, 2019). Those bimodal distributions are also seen in the contemporaneous clastic rocks of other forearc or trench-fill sedimentary units in the Northeast and Southwest Japan (e.g., Tokiwa *et al.*, 2019; Pastor-Galán *et al.*, 2021). This suggests that not only Jurassic but also Permian felsic igneous rocks were extensively distributed around the Asian continental margin during the deposition of these sandstones although they are not exposed in the Kitakami Mountains at present.

In the perspective of the geological structure, OM-07 and OM-06 are located between the sandstones from Locations 2 and 3 in Fig. 2, and the youngest cluster ages of OM-07 and OM-06 (183.3 ± 1.2 Ma and 176.7 ± 1.6 Ma, respectively) are also between them (191.9 ± 3.0 Ma of the sandstone in Location 2 and 164.8 ± 6.5 Ma in Location 3). Thus, the depositional ages of OM-07 and OM-06 are consistent with the geochronological trend of the Nakatsugawa Complex, where the ages become younger in a northeast direction (Uchino, 2019, 2021b).

The present study suggests that, in the Nakatsugawa Complex, the unit from the southwest margin to the location of OM-06 is an Early Jurassic accretionary complex, and its northeast part is a Middle Jurassic one (Fig. 2). However, it seems that the Nakatsugawa Complex were continuously formed during the Early to Middle Jurassic periods because there are no significant geochronological gap and lithological differences between the Early and Middle Jurassic parts.

7. Conclusion

Two sandstones (samples OM-07 and OM-06) were collected in the southwesternmost area of Iwaizumi Town, Iwate Prefecture, located on the southwestern margin of the North Kitakami Belt (Nakatsugawa Complex) for detrital zircon U–Pb dating. Both OM-7 and OM-06 show the youngest cluster ages of 183.3 ± 1.0 Ma and 176.7 ± 1.6 Ma, respectively, suggesting that they belong to the Early Jurassic accretionary complex.

The detrital zircon U–Pb data by this and previous studies clarified that the Nakatsugawa Complex appears to have been formed without the significant depositional-age gap.

Acknowledgements

We are grateful to Dr. Ogasawara, M. for his support during the LA-ICP-MS analysis. We would like to thank Drs. Watanabe, Y., Echigo, T., Muto, S. and Naya, T. for their careful and useful reviews.

This study was financially supported by the Japan Society for the Promotion of Science (JSPS) KAKENHI Grant Number 21K14005, 21H01174 and 19KK0091 (to S.A.) and JSPS KAKENHI Grant Number 19K04008 (to M.F.).

References

Brown, E. H. and Gehrels, G. E. (2007) Detrital zircon constraints on terrane ages and affinities and timing of orogenic events in the San Juan Islands and North Cascades, Washington. *Canadian Journal of Earth Sciences*, **44**, 1375–1396.

Corfu, F., Hanchar, J. M., Hoskin, P. W. O. and Kinny, P. (2003) An atlas of zircon textures. *Reviews in Mineralogy and Geochemistry*, **53**, 469–500.

Dickinson, W. R. and Gehrels, G. E. (2009) Use of U-Pb ages of detrital zircons to infer to maximum depositional ages of strata: A test against a Colorado Plateau Mesozoic database. *Earth and Planetary Science Letters*, **288**, 115–125.

Ehiro, M., Yamakita, S., Takahashi, S. and Suzuki, N. (2008) Jurassic accretionary complexes of the North Kitakami Belt in the Akka–Kuji area, Northeast Japan. *The Journal of Geological Society of Japan,* **114**, Supplement, 121–139 (in Japanese with English abstract).

Geological Survey of Japan, AIST (2022) Seamless digital geological map of Japan V2 1:200,000. https://gbank.gsj.jp/seamless (Accessed: 2022-7-20).

Han, R., Ree, J.-H., Cho, D.-L., Kwon, S.-T. and Armstrong, R. (2006) SHRIMP U–Pb zircon ages of pyroclastic rocks in the Bansong Group, Taebaeksan Basin, South Korea and their implication for the Mesozoic tectonics. *Gondwana Research*, **9**, 106–117.

Kim, S. W., Kwon, S., Ko, K., Yi, K., Cho, D., Kee, W. and Kim, B. C. (2015) Geochronological and geochemical implications of Early to Middle Jurassic continental adakitic arc magmatism in the Korean Peninsula. *Lithos*, **227**, 225–240.

Kiminami, K. and Imaoka, T. (2013) Spatiotemporal variations of Jurassic–Cretaceous magmatism in eastern Asia (Tan-Lu Fault to SW Japan): evidence for flat-slab subduction and slab rollback. *Terra Nova*, **25**, 414–422.

Matsuoka, A. (1988) Discovery of Early Jurassic radiolarians from the North Kitakami Belt (s. s.), northeast Japan. *Earth Science (Chikyu Kagaku)*, **42**, 104–106 (in Japanese with English abstract).

Nakae, S. and Kurihara, T. (2011) Direct age determination for an Upper Permian accretionary complex (Kirinai Formation), Kitakami Mountains, Northeast Japan. *Palaeoworld*, **20**, 146–157.

Okami, K. and Ehiro, M. (1988) Reviews and recent progress of studies on the Pre-Miyakoan sedimentary rocks of the Northern Kitakami Massif, Northeast Japan. *Earth Science (Chikyu Kagaku)*, **42**, 187–201 (in Japanese with English abstract).

Onuki, Y. (1956) Geology of the Kitakami Mountains. *In* Iwate Prefecture eds., *Explanatory Notes on the Geology of Iwate Prefecture, Part II*. p. 1–189. Iwate Prefecture, Morioka (in Japanese. title translated).

Pastor-Galán, D., Spencer, C. J., Furukawa, T. and Tsujimori T. (2021) Evidence for crustal removal, tectonic erosion and flare-ups from the Japanese evolving forearc sediment provenance. *Earth and Planetary Science Letters*, **564**, 116893.

Rubatto, D. (2002) Zircon trace element geochemistry: Partitioning with garnet and the link between U-Pb ages and metamorphism. *Chemical Geology*, **184**, 123–138.

Sagong, H., Kwon, S. and Ree, J. (2005) Mesozoic episodic magmatism in South Korea and its tectonic implication. *Tectonics*, **24**, TC5002.

Sharman, G. R. and Malkowski, M. A. (2020) Needles in a haystack: Detrital zircon U–Pb ages and the maximum depositional age of modern global sediment. *Earth-Science Reviews*, 103109.

Sláma, J., Košler, J., Condon, J. D., Crowley, J. L., Gerdes, A., Hanchar, J. M., Horstwood, M. S. A., Morris, G. A., Nasdata, L., Norberg, N., Shaltegger, U., Schoene, B., Tubrett, M. N. and Whitehouse, M. J. (2008) Plešovice zircon – A new natural reference material for U–Pb and Hf isotopic microanalysis. *Chemical Geology*, **249**, 1–35.

Suzuki, N., Ehiro, M., Yoshihara, K., Kimura, Y., Kawashima, G., Yoshimoto, H. and Nogi, T. (2007) Geology of the Kuzumaki–Kamaishi Subbelt of the North Kitakami Belt (a Jurassic accretionary complex), Northeast Japan: Case study of the Kawai–Yamada area, eastern Iwate Prefecture. *Bulletin of the Tohoku University Museum*, no. 6, 103–174.

Tokiwa, T., Shimura, Y., Takeuchi, M., Shimosato, S., Yamamoto, K. and Mori, H. (2019) Provenance of trench-fill deposits of the Jurassic Chichibu accretionary complex, Southwest Japan. *Journal of Asian Earth Sciences*, **184**, 103970.

Uchino, T. (2017) Late Triassic U–Pb–zircon age from tuffaceous mudstone in the Kadoma Complex, North Kitakami Belt, Northeast Japan. *The Journal of Geological Society of Japan*, **123**, 977–982 (in Japanese with English abstract).

Uchino, T. (2019) Detrital zircon U–Pb ages of sandstone within the Jurassic accretionary complex in the North Kitakami Belt of the Sotoyama District, Iwate Prefecture, Northeast Japan. *Bulletin of the Geological Survey of Japan*, **70**, 357–372 (in Japanese with English abstract).

Uchino, T. and Suzuki, N. (2020) Late Jurassic radiolarians

from mudstone near U–Pb-dated sandstone of the North Kitakami Belt in the northeastern Shimokita Peninsula, Tohoku, Japan. *Bulletin of the Geological Survey of Japan*, **71**, 313–330.

Uchino, T. (2021a) Recognition of an Early Triassic accretionary complex in the Nedamo Belt of the Kitakami Massif, NE Japan: New evidence of correlation with SW Japan. *Island Arc*, **30**, e12397. doi:10.1111/iar.12397

Uchino, T. (2021b) Middle Jurassic zircon age from sandstone within the accretionary complex in the North Kitakami Belt, Kamatsuda area in Iwaizumi Town, Iwate Prefecture, Northeast Japan: Verifying the age of the accretionary complex containing the Okawa Sample. *Bulletin of the Geological Survey of Japan*, **72**, 99–107 (in Japanese with English abstract).

Uchino, T. and Suzuki, N. (2021) Mesozoic radiolarian fossils from mudstone within the accretionary complex in the southwestern margin of the North Kitakami Belt, eastern Morioka, Iwate Prefecture, Northeast Japan. *Bulletin of the Geological Survey of Japan*, **72**, 119–127 (in Japanese with English abstract).

Uchino, T., Kawamura, M. and Kawamura, T. (2008) Lithology of the Nedamo Terrane, an Early Carboniferous accretionary complex, and its southern boundary with the South Kitakami Terrane. *The Journal of Geological Society of Japan*, **114**, Supplement, 141–157 (in Japanese with English abstract).

Ueda, H., Kimura, S., Saito, T., Takano, Y., Iizuka, N. and Orihashi, Y. (2018) Material recycling in a sediment-starved trench recorded in the Early Cretaceous Shiriya accretionary complex, Northeast Japan. *Island Arc*, **27**, e12272. doi:10.1111/iar.12272

Vermeesch, P. (2018) IsoplotR: a free and open toolbox for geochronology. *Geoscience Frontiers*, **9**, 1479–1493.

Wiedenbeck, M., Alle, P., Corfu, F., Griffin, W. L., Meier, M., Oberli, F., von Quadt, A., Roddick, J. C. and Spiegel, W. (1995) Three natural zircon standards for U–Th–Pb, Lu–Hf, trace element and REE analyses. *Geostandards Newsletter,* **19**, 1–23.

Recieved September 29, 2022
Accepted April 27, 2023

砕屑性ジルコン U–Pb 年代測定による北部北上帯中津川コンプレックスにおける前期及び中期ジュラ紀ユニット分布の制約

逢坂　将志・青木　翔吾・内野　隆之・福山　繭子

要　旨

北部北上帯南西縁に分布する中津川コンプレックスは，先行研究で報告された陸源性砕屑岩に含まれるジルコンの U–Pb 年代値や示準化石から，前期ジュラ紀と中期ジュラ紀の 2 つの付加体ユニットから構成されることが示唆されている．本研究では，両ユニットの分布をより詳細に制約するために，これまでに砕屑性ジルコン U–Pb 年代値が報告された地点の中で，地質構造的中間に位置する大川支流域の砂岩 2 試料 (OM-07 及び OM-06) について，砕屑性ジルコン U–Pb 年代測定を行った．その結果，前期ジュラ紀 (それぞれ 183.3 ± 1.0 Ma と 176.7 ± 1.6 Ma) の最若クラスター年代が得られた．本研究と先行研究から，本コンプレックスは南西縁部から OM-06 の分布域までが前期ジュラ紀，OM-06 よりも北東部が中期ジュラ紀に形成され，両者の間に有意な年代ギャップがないことが明らかにされた．

難読・重要地名

Sotoyama : 外山, Nakatsugawa : 中津川, Kuzumaki : 葛巻, Kamaishi : 釜石, Akka : 安家, Tanohata : 田野畑, Iwaizumi : 岩泉, Kadoma : 門馬, Todomatsu : 椴松, Hiegara : ヒエガラ (稗殻), Sannomata : 三ノ又, Okawa : 大川